Two-dimensional, unstructured mesh generation for tidal models

S. C. Hagen[a],*, J. J. Westerink[b], R. L. Kolar[c] and O. Horstmann[d]

[a] *Department of Civil and Environmental Engineering, University of Central Florida, Orlando, FL, U.S.A.*
[b] *Department of Civil Engineering and Geological Sciences, University of Notre Dame, Notre Dame, IN, U.S.A.*
[c] *School of Civil Engineering and Environmental Science, University of Oklahoma, Norman, OK, U.S.A.*
[d] *Brandenburg University of Technology, Cottbus, Germany*

SUMMARY

The successful implementation of a finite element model for computing shallow-water flow requires the identification and spatial discretization of a surface water region. Since no robust criterion or node spacing routine exists, which incorporates physical characteristics and subsequent responses into the mesh generation process, modelers are left to rely on crude gridding criteria as well as their knowledge of particular domains and their intuition. Two separate methods to generate a finite element mesh are compared for the Gulf of Mexico. A wavelength-based criterion and an alternative approach, which employs a localized truncation error analysis (LTEA), are presented. Both meshes have roughly the same number of nodes, although the distribution of these nodes is very different. Two-dimensional depth-averaged simulations of flow using a linearized form of the generalized wave continuity equation and momentum equations are performed with the LTEA-based mesh and the wavelength-to-gridsize ratio mesh. All simulations are forced with a single tidal constituent, M_2. Use of the LTEA-based procedure is shown to produce a superior (i.e., less error) two-dimensional grid because the physics of shallow-water flow, as represented by discrete equations, are incorporated into the mesh generation process. Copyright © 2001 John Wiley & Sons, Ltd.

KEY WORDS: localized truncation error analysis; shallow-water flow; tidal model; grid generation

1. INTRODUCTION

Recent advances in surface water modeling have permitted the development and successful implementation of coastal ocean circulation models for increasingly larger domains [1–9]. While a large domain increases the predictive capabilities of coastal ocean models [9,10], it complicates the process of node placement. Large domains require a strategic placement of nodes in order to maintain acceptable levels of local and global accuracy for a given

---

* Correspondence to: Department of Civil and Environmental Engineering, University of Central Florida, College of Engineering, PO Box 162450, Orlando, FL 32816-2450, U.S.A.

computational cost. In this paper, the process of computational node placement will be discussed and a method of grid generation will be presented which more successfully couples the physics, as represented by discrete equations, underlying tidal flow and circulation to the mesh generation process.

Larger domains warrant a method of gridding that utilizes unstructured meshes, e.g., the finite element method, which allows for spatially varying levels of resolution. Since, in general, shallower water has a higher localized wave number content than deeper water, greater resolution will be required in shallow water regions. Furthermore, it has been shown that the computed response is highly sensitive to grid resolution in regions with steep bathymetric gradients [11–14]. Two-dimensional response structures associated with intricate shorelines, two-dimensional topography, amphidromes (a point from which all co-tidal lines radiate), and resonant bays also require local refinement of grids. Conversely, deep ocean waters usually result in large expanses with more slowly varying response structures in space, which can utilize a coarser level of resolution. These considerations indicate that variably graded meshes are needed, which are easily implemented with the finite element method.

The method of producing variably graded meshes in currently poorly defined, imprecise and *ad hoc*. It is a tedious process at best. Since no robust criterion or node spacing routine exists that incorporates the aforementioned physical characteristics and subsequent responses into the mesh generation process, modelers are left to rely on crude and entirely localized node placement criteria, such as the wavelength-to-gridsize ratio, and on their knowledge of particular domains as well as their intuition. The mesh generation process prohibits the fully automatic production of an unstructured grid, which hinders the fast application of the finite element method to large-scale problems.

It is proposed in this paper that a localized truncation error analysis (LTEA), an *a posteriori* error estimation procedure, can be used to optimally place nodes in two-dimensional domains. A simplified case (single constituent forcing, linear constant friction, and no Coriolis) is presented herein as a stepping-stone to developing grids for more complicated scenarios. The LTEA is applied to the actual discretized equations and includes approximations to the variables being simulated and their derivatives. Thus, an LTEA-based node placement routine directly couples the estimated truncation errors to the actual mesh generation process.

Three variably graded grids are developed for the Gulf of Mexico model domain. One mesh is based on the wavelength-to-gridsize ratio [10]

$$\frac{\lambda}{\Delta} = \frac{\sqrt{gh(x, y)}}{\Delta(x, y)} T \tag{1}$$

where g is the gravitational constant, $h(x, y)$ is the water depth, T is the tidal period of interest, and $\Delta(x, y)$ is the the gridsize, e.g., the side-length of a triangle, with x and y representing the Cartesian co-ordinate location. The ratio is set to some a constant value, usually 40 or less, and a grid is generated with the aid of this criterion [10]. A second grid is produced by means of a LTEA, wherein local element sizes are adjusted such that truncation error is held at a constant value throughout the domain. A third mesh is generated by splitting each triangular element of the LTEA-based grid into four triangular elements. Each of the three grids is utilized in a linear simulation of 15 days of real time, which is forced with the M_2 tidal

constituent. Error properties are compared by interpolating the responses from the wavelength-based and LTEA-based grids onto the split-by-four LTEA-based grid and then subtracting the responses from the split-by-four grid. The paper concludes with a discussion of the results and a comparison of these two methods with regards to the Gulf of Mexico model domain.

2. GULF OF MEXICO MODEL DOMAIN AND FORMULATION

Figure 1 defines the Gulf of Mexico (GOMEX) domain and provides bathymetric contours. The GOMEX domain is chosen because it presents a true test of the LTEA-based methodology for four major reasons. First, the GOMEX domain is a larger-scale domain encompassing approximately 1.5 million km^2, and thus requires a graded mesh. Second, high gradients of bathymetry and well-defined shelf regions are present. Third, by simulating the entire GOMEX, two well-defined open ocean boundaries of limited extent provide the boundary forcing. Fourth, this basin contains complex two-dimensional flow structures, an amphidrome, and shelf resonant features, all of which provide a shallow-water modeling challenge [10].
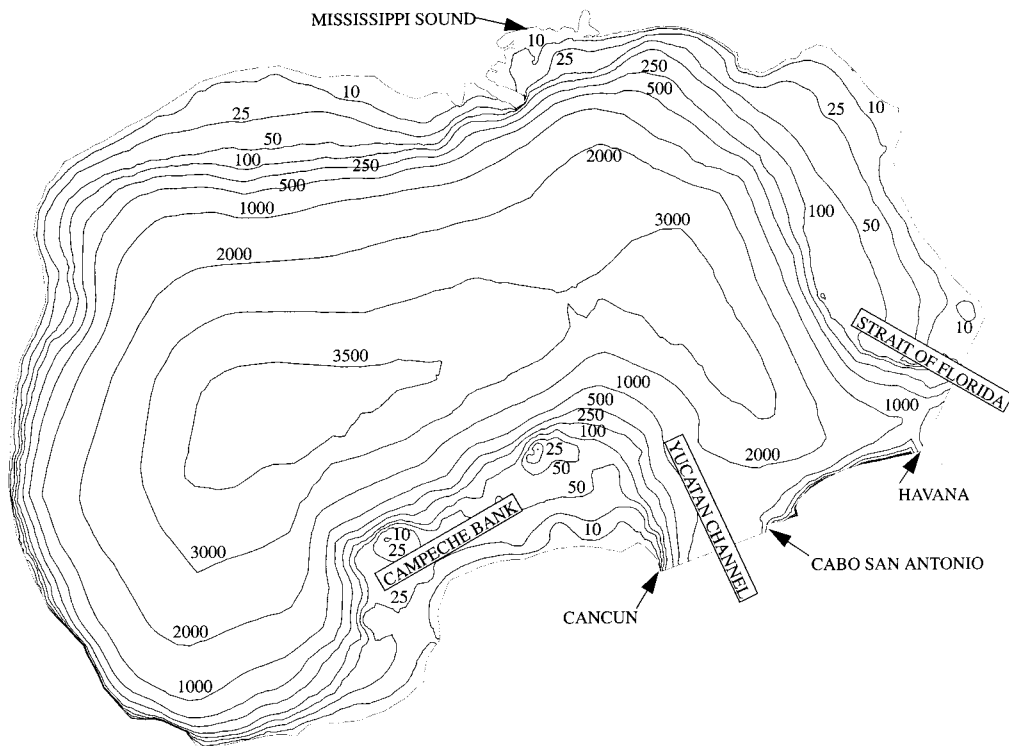

Figure 1. GOMEX model domain with bathymetric contours (meters).

Most of the bathymetric data was originally obtained from the ETOPO5 database from the National Center for Atmospheric Research [15]. In addition, the National Oceanic and Atmospheric Administration (NOAA) Digital U.S. Coastal Hydrography sounding database (distributed by NOAA National Geophysical and Solar–Terrestrial Data Center, Boulder, CO, U.S.A.) is used from the Mississippi Sound to St. Marks, FL. A minimum bathymetry of 3.0 m is specified for all linear simulations. The two open ocean boundaries include the Yucatan Channel and the Strait of Florida (Figure 1). Sea surface elevations are enforced at each of these boundaries and the M_2 frequency is used as the sole tidal constituent. The first open boundary stretches across the Yucatan Channel from the vicinity of Cancun, Mexico, to Cabo San Antonio, Cuba. The second open boundary runs across the Strait of Florida, beginning at Havana, Cuba, and proceeding in a straight path to Cape Sable, FL. Sea surface elevation boundary conditions for the M_2 tidal constituent are extracted for both open ocean boundaries from the Western North Atlantic Tidal Model Database [16]. Because of the domain size, 1.5 million km^2, tidal potential terms are included for the M_2 tidal constituent.

The two-dimensional computations that are used to generate two-dimensional LTEA-based grids are realized with a finite element model of the linearized shallow equations. There are two main reasons that justify using a linear form of the shallow-water equations. First, shallow-water modeling of a long-wave process in a large basin is weakly non-linear. Because the contribution from the non-linear terms is minimal, examination of the truncation error associated with the linear form of the shallow-water equations should produce a finite element grid that will be suited for non-linear simulations. Second, the concept of mesh generation that is based on multiple orders of the truncation error series is in the early stages of research. Simplicity, herein in the form of the linearized shallow-water equations, will help facilitate a clear understanding of the details and implications of this theory. In addition, simplicity will also lead to a streamlined process, which is important for an efficient algorithm.

All simulations in this paper are performed with ADCIRC-2DDI, a two-dimensional depth-integrated hydrodynamic circulation code [5,15]. The governing equations that are solved consist of the generalized wave continuity equation (GWCE) and the momentum equations. The continuity equation is in fact replaced by the GWCE [3,5]. The linearized two-dimensional GWCE is given by

$$\frac{\partial^2 \eta}{\partial t^2} + \tau_0 \frac{\partial \eta}{\partial t} - g \left[\frac{\partial}{\partial x} \left(h \frac{\partial \eta}{\partial x} \right) - \frac{\partial}{\partial y} \left(h \frac{\partial \eta}{\partial y} \right) \right] - (\tau - \tau_0) \left[\frac{\partial}{\partial x} (uh) - \frac{\partial}{\partial y} (vh) \right] = 0 \tag{2}$$

and the two-dimensional, linearized, non-conservative momentum equations are expressed as

$$\frac{\partial u}{\partial t} + g \frac{\partial \eta}{\partial x} + \tau u = 0 \tag{3}$$

$$\frac{\partial v}{\partial t} + g \frac{\partial \eta}{\partial y} + \tau v = 0 \tag{4}$$

where t is the time, x and y are spatial co-ordinates, η is the deviation of the free surface from the geoid, u is the depth-averaged velocity in the x-direction, v is the depth-averaged velocity

in the y-direction, τ_0 is a weighting parameter in the GWCE that controls the contribution from primitive continuity (in the limit, as $\tau_0 \Rightarrow \infty$, GWCE $\Rightarrow$ primitive continuity), g is the gravitational acceleration, h is the depth below the geoid, and τ is the linear bottom friction coefficient. ADCIRC-2DDI applies linear, Galerkin, triangular finite elements.

All simulations are linear and use a constant bottom friction coefficient of 0.0004 and a GWCE weighting parameter (τ_0) of 0.0004 [13,14]. A no-flow boundary condition is enforced at all land boundaries and open ocean boundaries are forced as discussed above. Fifteen days of real time are simulated with each grid to ensure that a dynamic steady state is achieved. A time step of 90 s is used for coarse grids and 45 s for the fine grid. A hyperbolic ramping function is imposed during the first two days [5].

3. A GOMEX WAVELENGTH-BASED FINITE ELEMENT GRID

A wavelength-to-gridsize ratio grid is developed by employing Equation (1) with the bathymetry for the GOMEX domain [17]. Equation (1) is set equal to a target wavelength-to-gridsize ratio of 100, which is conservative when compared with commonly used values reported in the literature [10], and an M_2 tidal period of 12.42 h is used. The allowable node spacings for the wavelength-based mesh may then be computed with

$$\Delta(x, y) = \frac{\sqrt{gh(x, y)}}{R_{\text{target}}} T \tag{5}$$

where the side-length of a triangular element is taken as $\Delta(x, y)$ and the bathymetry value $h(x, y)$ is interpolated at the geometric center of each triangular element. Of course, as the element size is not a continuous function in a mesh, the desired target ratio (R_{target}) of 100 will not be met exactly in the final mesh. Therefore, a tolerance bandwidth of acceptable wavelength-to-gridsize ratios is defined as $70 < R_{\text{target}} < 130$.

The final wavelength-based mesh, which will henceforth be referred to as GOMEX_W100 (Figure 2), is a finite element grid with 33 272 triangular elements and 17 306 nodes. The range of the node spacing varies from approximately 1.0 to 125 km. The mesh has a nodal average of wavelength-to-gridsize ratio that falls between 70 and 130.

A simulation using GOMEX_W100 is performed with ADCIRC [5,15] as detailed in the previous section. The results are harmonically analyzed from day 12 through to day 15 to produce the elevation and x- and y-direction velocity amplitudes and phases for the M_2 tidal constituent. The elevation amplitude ranges from 0.0 to 29 cm; the velocity amplitudes range from 0.0 to 120 cm s^{-1}.

4. AN LTEA FOR THE GOMEX MODEL DOMAIN

Truncation error is developed and estimated for a finite element grid that is assumed to have equilateral, triangular elements on a local scale [13] (as represented by Figure 3). Equilateral elements are desired because rapidly changing element sizes, i.e., skewed elements, result in
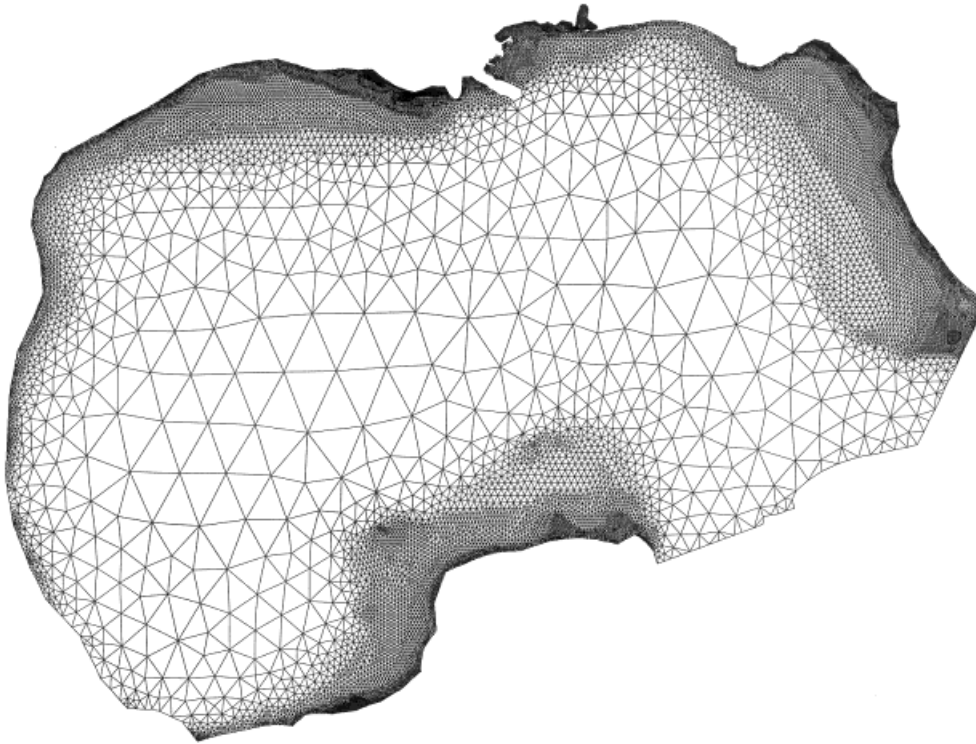
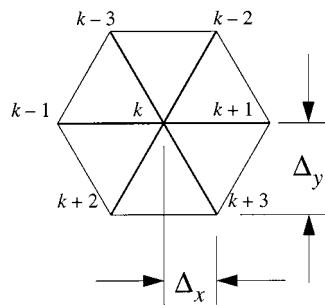Figure 2. GOMEX_W100: wavelength-based graded mesh for the GOMEX.

Figure 3. A typical interior node, k, and the nodes surrounding it for a valence of six.

higher odd-order truncation error terms [14], different sets of cross-derivative terms in the two-dimensional truncation error series and poorly behaved transformation functions [18]. The assumption permits (1) an estimation of truncation error for the finite element grid that is being developed; (2) that Δ_y may be expressed as a function of Δ_x, i.e., $\Delta_y = \sqrt{3}\Delta_x$. Note that the assumption of equilateral triangular elements would be approximated locally throughout a given finite element grid. However, since the grids that are generated will be unstructured, the assumption cannot be valid globally, although the assumption will be valid locally provided element sizes do not change too rapidly.

Note that all local truncation errors and local node spacing requirements presented herein are estimated using only the truncation error associated with the non-conservative momentum equations [13,14]. Five reasons are given for this:

1. The GWCE formulation incorporates momentum.
2. The non-conservative momentum equation is simpler to work with than the GWCE. This means fewer computations are required to compute local truncation error and, subsequently, to generate node spacing requirements. In addition, the method of LTEA-based grids has good potential for adaptive mesh refinement, which requires fast error calculations.
3. The non-conservative momentum equation does not include h, the depth from the geoid. While it may be argued that this is precisely why the GWCE should be incorporated, that logic misses the key reason for pursuing this method of grid generation, i.e., a desire to develop a method of grid generation that is directly related to the response, as represented by the dependent variables η, u, and v.
4. Not all modelers use GWCE-based shallow-water equations. Therefore, the approach taken herein will have a wider appeal.
5. Extensive development and testing in one-dimensional applications indicated that results are satisfactory [13,14].

Because the truncation error is developed for a specific configuration, i.e., six equilateral elements surrounding the local node (Figure 3), sixth- and higher-order terms are truncated and the lower-order terms solved for Δ, noting that $\Delta = \Delta_x$. This provides an estimate of the second- and fourth-orders of truncation error associated with the discrete form of the linear, harmonic, non-conservative momentum equations on the interior nodes of an equilateral triangular grid [13]

$$
\begin{aligned}
\tau_{ME} = \Delta^2 & \left[\left(\frac{\hat{i}\omega + \tau}{2} \right) \left(\frac{\partial^2 \hat{u}_k}{\partial x^2} + \frac{\partial^2 \hat{v}_k}{\partial x^2} + \frac{\partial^2 \hat{u}_k}{\partial y^2} + \frac{\partial^2 \hat{v}_k}{\partial y^2} \right) + \frac{g}{2} \left(\frac{\partial^3 \hat{\eta}_k}{\partial x^3} + \frac{\partial^3 \hat{\eta}_k}{\partial x^2 \, \partial y} + \frac{\partial^3 \hat{\eta}_k}{\partial x \, \partial y^2} + \frac{\partial^3 \hat{\eta}_k}{\partial y^3} \right) \right] \\
+ \Delta^4 & \left[\left(\frac{\hat{i}\omega + \tau}{8} \right) \left(\frac{\partial^4 \hat{u}_k}{\partial x^4} + \frac{\partial^4 \hat{v}_k}{\partial x^4} + 2 \frac{\partial^4 \hat{u}_k}{\partial x^2 \, \partial y^2} + 2 \frac{\partial^4 \hat{v}_k}{\partial x^2 \, \partial y^2} + \frac{\partial^4 \hat{u}_k}{\partial y^4} + \frac{\partial^4 \hat{v}_k}{\partial y^4} \right) \right. \\
& \left. + \frac{g}{24} \left(\frac{22}{10} \frac{\partial^5 \hat{\eta}_k}{\partial x^5} + \frac{\partial^5 \hat{\eta}_k}{\partial x^4 \, \partial y} + 2 \frac{\partial^5 \hat{\eta}_k}{\partial x^3 \, \partial y^2} + 6 \frac{\partial^5 \hat{\eta}_k}{\partial x^2 \, \partial y^3} + 3 \frac{\partial^5 \hat{\eta}_k}{\partial x \, \partial y^4} + \frac{9}{5} \frac{\partial^5 \hat{\eta}_k}{\partial y^5} \right) \right]
\end{aligned}
\tag{6}
$$

where $\hat{u}$, $\hat{v}$, and $\hat{\eta}$ are complex amplitudes of u, v, and η; g is the gravitational constant; τ is the bottom friction coefficient, $\hat{i} = \sqrt{-1}$; ω is the response frequency; and k is the center node in Figure 3.

Central difference approximations for a regular grid ($\Delta x = \Delta y$) are employed to estimate the partial derivatives of Equation (6). These are carefully developed such that the estimates of the second- and third-order partial derivatives have a leading-order accuracy of order four and the fourth- and fifth-order partial derivatives have a leading-order accuracy of order two. Compilation of the central difference approximations results in a 9×9 central differencing molecule, wherein all derivative estimations span the molecule [13].

The local application of the 9×9 central differencing molecule requires that harmonic solutions from a base finite element solution be interpolated onto the molecule as it is applied to interior nodes of the base grid. Each node of the finite difference molecule must fall within a different element in order to maintain the integrity of the finite difference approximations, since on an elemental level these high-order derivatives are equal to zero.

To generate the base finite element solution, a uniform mesh (GOMEX_UNIFORM) is developed for the GOMEX model domain using the boundary of GOMEX_W100 and equilateral triangular elements on the interior with a uniform side length of 3000 m (resulting in nearly 170000 nodes) [17]. The bathymetry of GOMEX_W100 is interpolated onto this uniform mesh and a linear simulation is performed as detailed in Section 2. The results are harmonically analyzed from day 12 through to day 15 to produce the elevation and x- and y-direction velocity amplitudes and phases for the M_2 tidal constituent.

It should be noted that a highly resolved uniform mesh is only required for a single linear simulation of limited duration. This initial linear run is relatively quick to perform, especially when compared with long-term non-linear simulations that may be performed with the unstructured grid and can involve multiple scenarios, e.g., hindcasting and forecasting. In fact, this single simulation can be performed independent of time, i.e., by using a discrete form of the linear, harmonic equations for shallow-water flow. Further, the approach permits an *a posteriori* assimilation of large bathymetric datasets by using a fine-resolution mesh to perform a preliminary linear simulation. It is also noted that one could follow these strategies to generate LTEA from crude grids and then refine with an iterative approach.

The 9×9 central differencing molecule is employed with the linear, harmonic results from GOMEX_UNIFORM to estimate the second- and fourth-orders of truncation error of Equation (6). Figure 4 shows the local truncation error estimate. Note that use of the 9×9 central differencing molecule does not permit an estimate of the local truncation error up to the boundaries. The truncation error ranges from a peak value of 9.82×10^{-7}, found at the Strait of Florida (see Figure 1 for the location of particular regions) to 2.47×10^{-13} in the deep regions. Near-peak values are also seen in the following areas: throughout the Mississippi Sound region; extending west of the Yucatan Channel on the Campeche Bank; scattered along the shelf breaks; all along the Florida Shelf. A remarkable concentration of a high level of local truncation error is seen at the Strait of Florida, and extends west and then north into the domain. In all cases, this local rise in truncation error directly corresponds with high gradients in the elevation and velocity fields, and does not necessarily correspond to high gradients of bathymetry.
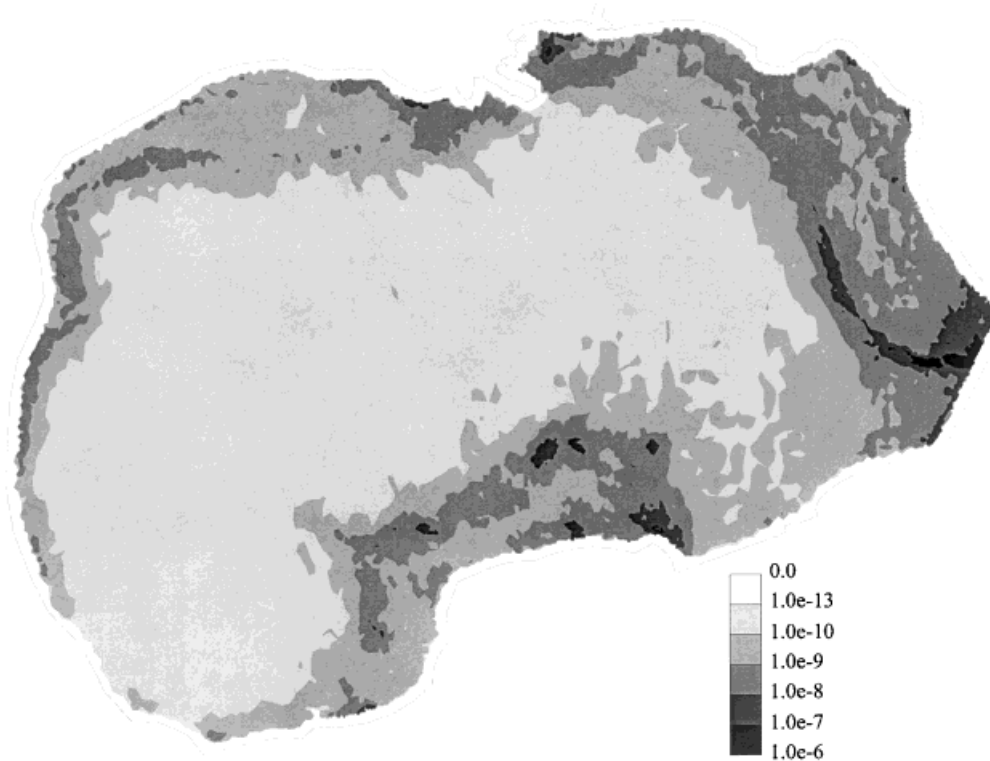
Figure 4. Second- and fourth-order local truncation error (m s^{-2}) from the two-dimensional momentum equations with the GOMEX domain.

5. AN LTEA-BASED FINITE ELEMENT GRID FOR THE GOMEX DOMAIN

A scalar value, which represents the maximum allowable finite element spacing, is computed at each node of the uniform grid by setting Equation (6) equal to the peak local truncation error value, 9.82×10^{-7}. The complex quadratic is solved for Δ with the minimum real root selected as the scalar value; it is used to define a radius of maximum allowable finite element spacing. This procedure is carried out for each interior node of the GOMEX_UNIFORM grid. The local node spacing requirements are changed at all but one location as a result of forcing the truncation error to be constant, with the node where the peak local truncation error is attained being the one exception.

Figures 5 and 6 presents contour plots of radii of maximum allowable finite element spacings for the GOMEX domain. The entire domain is shown in Figure 5 and two details for the Strait of Florida are provided in Figure 6. Local node spacing requirements range from a minimum of 3 km at the Strait of Florida, where the peak truncation error is located, to a maximum of approximately 120 km, which can be found throughout the deeper regions. Since
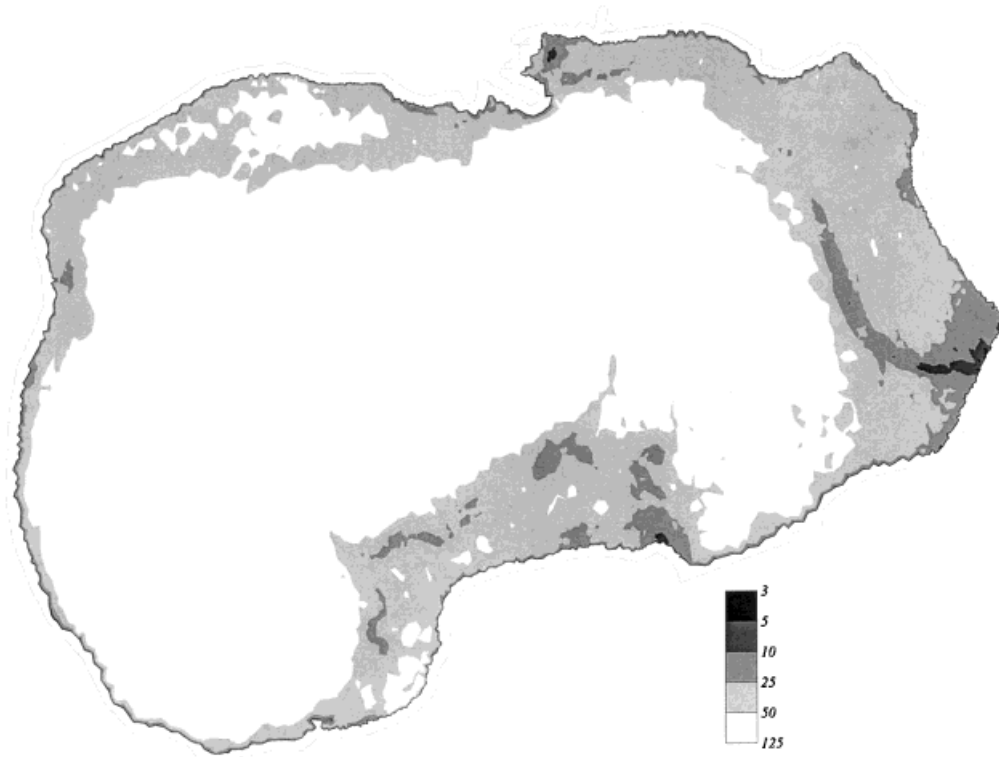
Figure 5. Radii of maximum allowable finite element spacings for the GOMEX (in km) which are based on the second- and fourth-orders of local truncation error from the two-dimensional momentum equations.

the goal is to hold truncation error at a constant level, the local node spacing requirements mirror the truncation errors that are shown in Figure 4.

The scalar values from the above operations are employed to produce an LTEA-based finite element grid [17]. Since no LTEA-based spacing requirements are computed near shore, the GOMEX_W100 boundary and near-shore elements are used to ensure comparability with the wavelength-based mesh. In addition, the LTEA-based spacing requirements are multiplied by a scaling factor such that the final total number of nodes is approximately 17000—the same as the GOMEX_W100 grid. For this application a factor of 0.29 was used to arrive at approximately 17000 nodes.

The end result is a finite element grid (GOMEX_LTEA; Figure 7) with 33 727 triangular elements and 17 541 nodes as compared with the 33 272 triangular elements and 17 306 nodes of GOMEX_W100. The range of the node spacing varies from approximately 0.7 to 40 km, as compared with 1.0 to 125 km for the wavelength-based grid. Two details of the LTEA-based mesh are also shown in Figure 6 to substantiate that the mesh closely follows the spacing
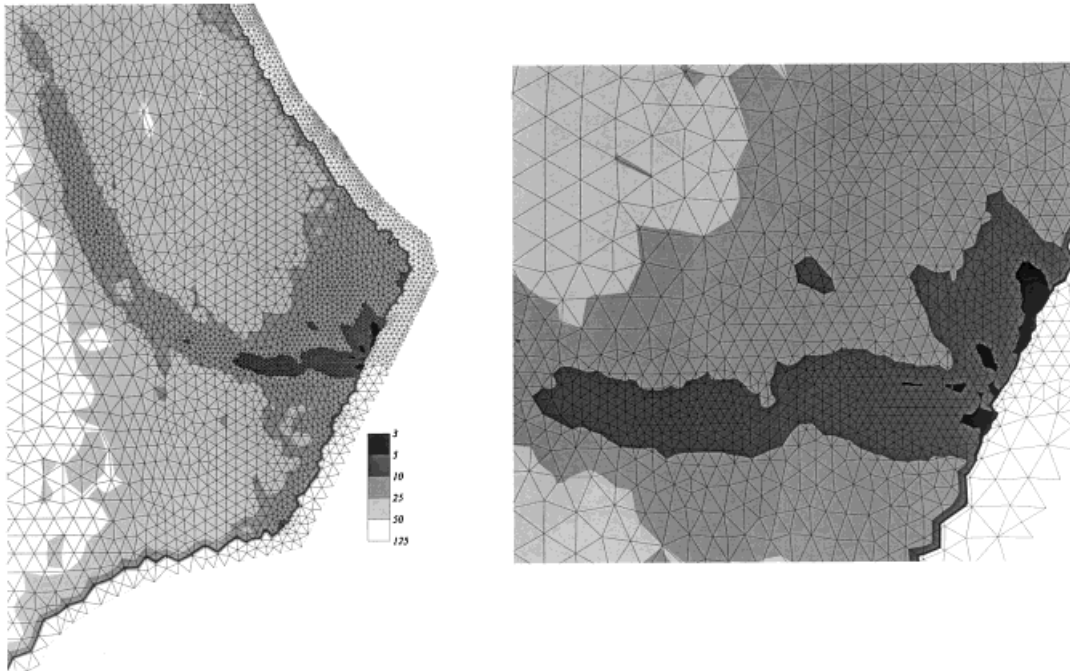
Figure 6. Details of the spacing requirements for the GOMEX in the Strait of Florida region.

requirements. Simulation errors associated with the LTEA-based grid may be contrasted with GOMEX_W100, since GOMEX_LTEA has approximately the same total number of nodes and uses boundary, bathymetry, and near-shore elements from GOMEX_W100.

Comparison of the LTEA-based finite element grid (Figure 7) to the wavelength-based grid (Figure 2) yields the following observations. On the whole, GOMEX_LTEA provides a smoother transition in element sizes from the shoreline to the deep ocean. While the wavelength-based grid provides the finest resolution adjacent to the coast and fine resolution out to the shelf breaks, the LTEA-based grid has more resolution at the shelf break, allows for a relaxation in resolution on the shelf, and then provides a fine resolution near shore. The shelf break resolution is a characteristic that was observed with one-dimensional LTEA-based grids [13,14]. Note the shelf break region near the Strait of Florida, which has a dramatic rise from the deep region to the shelf break (Figures 1 and 7). For this region, the LTEA-based method promotes a gradual variation in element sizes where elevation and velocity amplitudes have high gradients. The GOMEX_LTEA grid provides a resolution of 0.7–6.0 km in the region off the Strait of Florida, where the elevation and velocity amplitude gradients are also high, whereas the GOMEX_W100 node spacing ranges from approximately 2.7 to 25.0 km.

Two simulations are performed with ADCIRC [5,15] on LTEA-based grids. The first applies the basic LTEA grid just described, GOMEX_LTEA. The second utilizes a refined version of
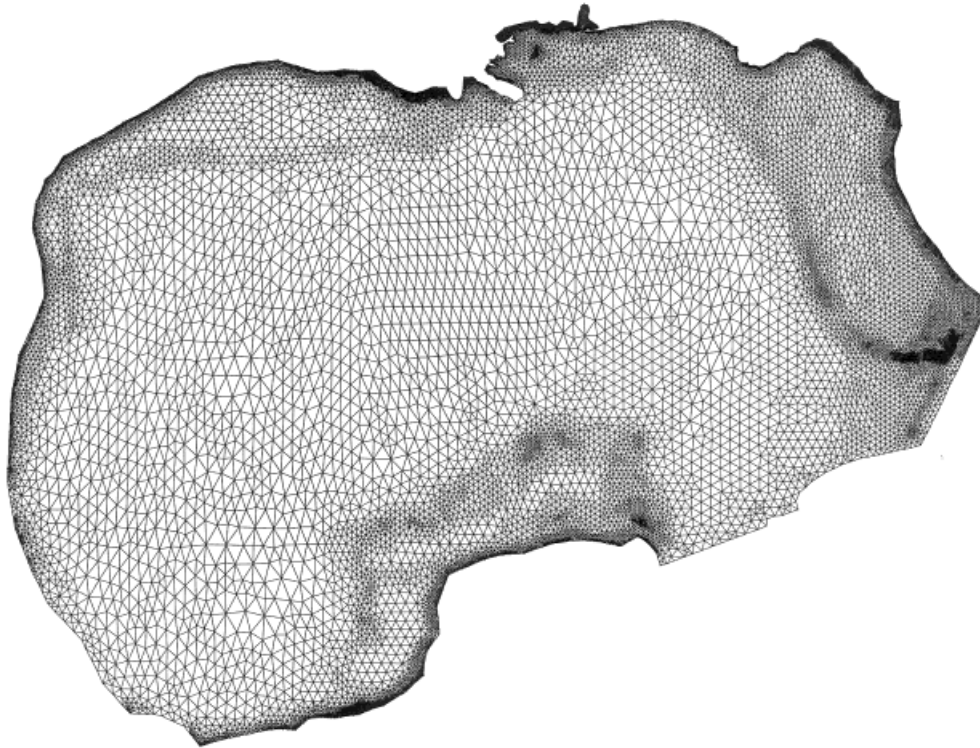
Figure 7. An LTEA-based finite element grid for the GOMEX.

this basic LTEA grid, which is GOMEX_LTEA with each triangular element split by four. The second simulation provides a basis for estimating errors for both the LTEA and wavelength-to-gridsize results. The results are harmonically analyzed from day 12 to day 15 to produce the elevation and x- and y-velocity amplitudes and phases for the M_2 tidal constituent.

6. ESTIMATED ERROR COMPARISONS AND DISCUSSION

The harmonic results are used to examine the error properties associated with finite element grids produced using the wavelength-to-gridsize ratio and an LTEA. This is achieved by measuring the error between coarse and fine grid results. Absolute errors are computed as

$$\varepsilon_A(x, y) = \left| A_c(x, y) - A_f(x, y) \right| \tag{7}$$

with $A_c(x, y)$ the coarse grid solution, and $A_f(x, y)$ the fine grid solution. Relative errors are normalized and expressed as a percentage

$$\varepsilon_R(x, y) = \frac{\varepsilon_A(x, y)}{A_f(x, y)} 100 \tag{8}$$

Velocity errors are presented with respect to one tidal cycle. During one tidal cycle, at each node, the velocity vector traces out an ellipse that can be described by five components: the major and minor axis, the phase lag, the eccentricity, and the major semi-axis direction. The lengths of the major semi-axis and minor semi-axis equal the maximum and minimum current respectively during the tidal cycle. The phase lag is the angle that the maximum current vector lags the astronomical forcing. The eccentricity of an ellipse is the ratio of the distance between the foci to the length of the major axis. The major semi-axis direction is the angle of inclination that the major semi-axis makes with the positive x-axis.

Cumulative area fraction error (CAFE) [12] curves are used to display the errors for the grid generation study (Figures 8–10). The CAFE plots present under- and overprediction errors versus a cumulative percentage of the total area exceeded by the respective error. Note that a perfect solution would result in a single vertical line plotted at zero on the x-axis. For reference purposes, each plot has a horizontal line at a value equal to 1 per cent of the cumulative area. The x-co-ordinate where the horizontal line intersects the curve displays the error levels exceeded within 1 per cent of the total domain. Note that the error levels associated with 99 per cent of the total domain area are plotted above the horizontal line.

Figure 8(a)–(c) presents the absolute and relative elevation amplitude errors and the absolute elevation phase errors. Figure 9(a)–(c) shows the absolute and relative major semi-axis errors and the absolute major semi-axis phase error. Figure 10(a) and (b) displays the absolute eccentricity and absolute major semi-axis direction errors. A dramatic difference in all error levels is seen throughout the domain when considering the wavelength results (solid line) versus the LTEA results (dashed line). Also note the symmetry of the LTEA results, which shows consistency on under- and overprediction errors above the horizontal line at 1 per cent in Figures 8–10.

Tables I and II provide specific error levels from the CAFE plots. Table I highlights elevation error results and Table II contains velocity error information. Each of the eight categories in Tables I and II contains three error measures for the GOMEX_LTEA and GOMEX_W100 grids. The error measures are: percentage of the total domain area that exceeds a certain underprediction of error; percentage of the total domain area that exceeds a certain overprediction of error, total per cent of the area that exceeds the error band formed by this under- and overprediction of error. The bold values in Tables I and II highlight the lowest error measures. In every category the bold value is in the GOMEX_LTEA column. The gain in accuracy by utilizing the LTEA-based approach is 34–43 times better than the wavelength-to-gridsize approach when considering the total elevation error band measures of Table I. The velocity error band measures in Table II show between a three- and sixfold improvement in accuracy for the LTEA-based approach. In short, Figures 6–8 and Tables I and II clearly demonstrate that the LTEA-based grid significantly outperforms the wavelength-to-gridsize ratio mesh in all error measures.
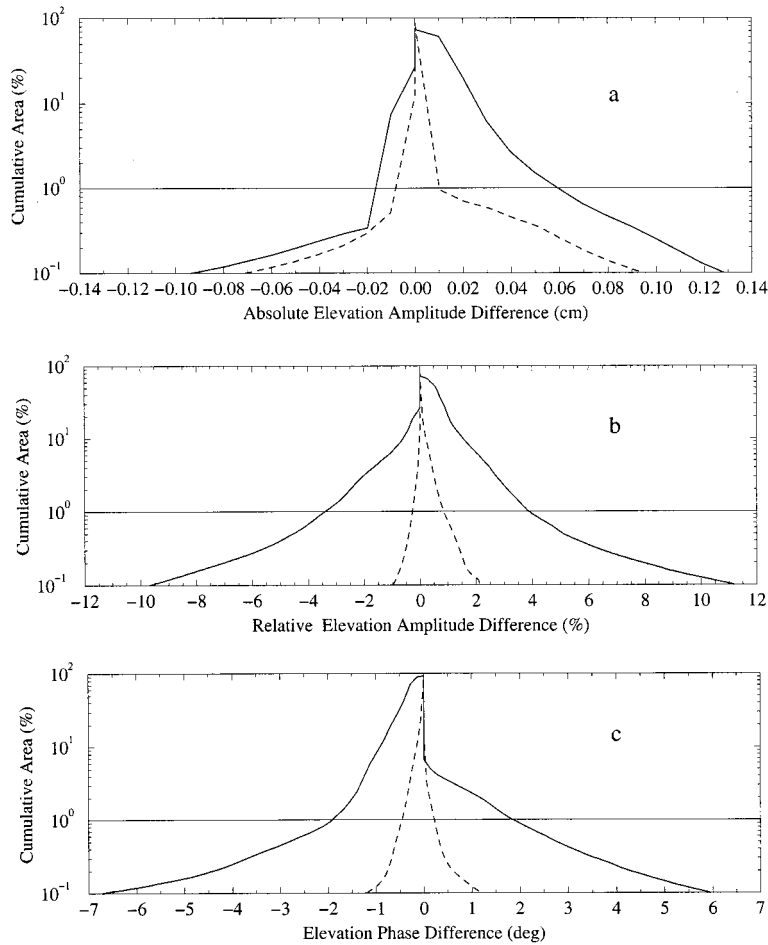
Figure 8. GOMEX_W100 (solid curve) and GOMEX_LTEA (dashed curve) CAFE plots of elevation errors: (a) absolute elevation amplitude; (b) relative elevation amplitude; (c) absolute elevation phase.

A very simplified case (M_2 forcing only, linear constant friction, and no Coriolis) has been presented in order to compare the LTEA-based approach with the wavelength-based criterion. However, it is noted that there are substantial differences in response functions for different tidal constituent species (e.g., non-semi-diurnals) [10] and one can presume changes in the LTEA and subsequent changes in the grid design. Further, an introduction of non-linear friction and the Coriolis term will also alter the momentum balance and lead to changes in the LTEA-based mesh. It is noted that all of these considerations can be readily included in future modifications to the LTEA.
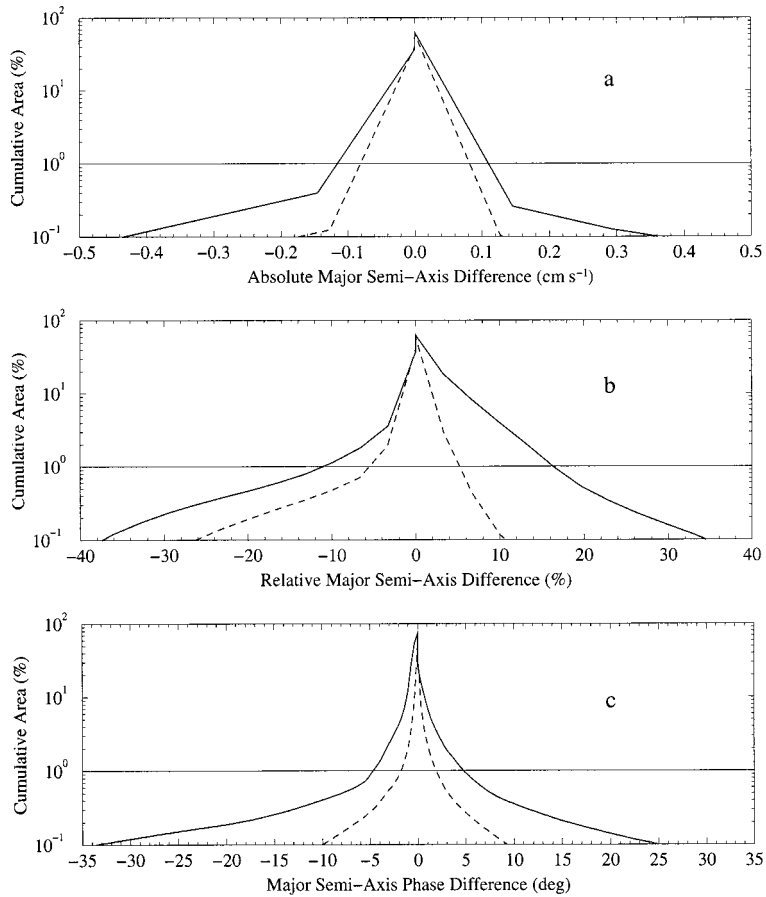
Figure 9. GOMEX_W100 (solid curve) and GOMEX_LTEA (dashed curve) CAFE plots of velocity errors: (a) absolute major semi-axis; (b) relative major semi-axis; (c) absolute major semi-axis phase.

7. CONCLUSIONS

The LTEA-based approach searches out high gradients in the response function (elevation and velocity fields in the example) and adds resolution where it is needed. The GOMEX_LTEA grid shows that grid design should be quite different than what the wavelength-to-gridsize ratio promotes. The GOMEX_W100 grid is very fine near shore and coarse in the deep waters. GOMEX_LTEA is coarser on the shelf, provides fine resolution at the shelf break and near other steep bathymetric gradients, and is finer in the deep regions than GOMEX_W100. Many of the resolution differences between the LTEA-based approach and the wavelength-to-gridsize ratio are in areas where there are high gradients in the elevation and velocity fields, but not necessarily high gradients of bathymetry, e.g., the deep regions and the Strait of Florida. The
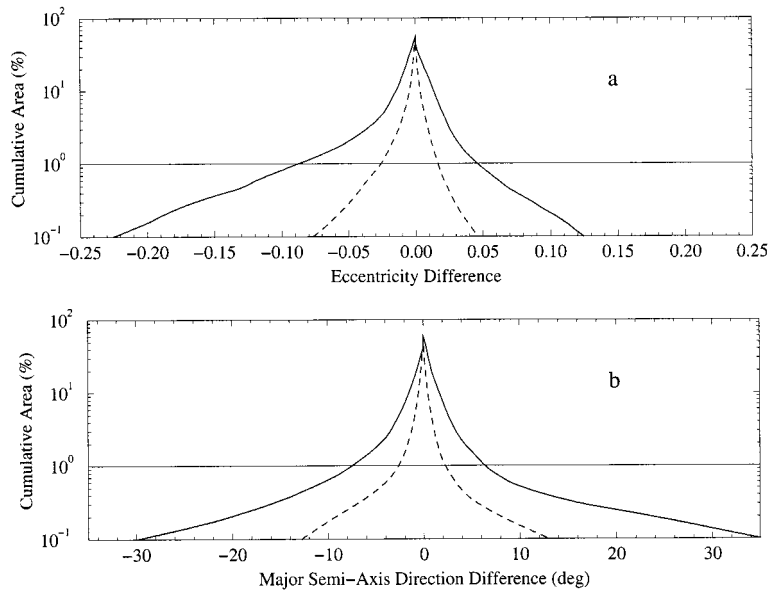
Figure 10. GOMEX_W100 (solid curve) and GOMEX_LTEA (dashed curve) CAFE plots of velocity errors: (a) absolute eccentricity; (b) absolute major semi-axis direction.

Table I. Elevation error measures, relative to the split-by-four version of the LTEA-based grid.

	GOMEX_LTEA	GOMEX_W100
Elevation amplitude (absolute)		
Per cent area exceeding -0.01 cm	**0.54**	7.27
Per cent area exceeding $+0.01$ cm	**1.04**	60.07
Total per cent area exceeding ± 0.01 cm	**1.58**	67.34
Elevation amplitude (relative)		
Per cent area exceeding -1.0%	**0.10**	6.54
Per cent area exceeding $+1.0\%$	**0.71**	21.13
Total per cent area exceeding $\pm 1.0\%$	**0.81**	27.67
Elevation phase (°)		
Per cent area exceeding $-1.0°$	**0.12**	7.99
Per cent area exceeding $+1.0°$	**0.12**	2.34
Total per cent area exceeding $\pm 1.0°$	**0.24**	10.33

wavelength-to-gridsize ratio criterion displays its limitations, i.e., resolution is a function of bathymetry only. In addition, the two-dimensional finite element grid that is based on LTEA promotes a smooth transition in resolution from the deep regions to the shelf breaks and then

Table II. Velocity error measures, relative to the split-by-four version of the LTEA-based grid.

	GOMEX_LTEA	GOMEX_W100
Major semi-axis (absolute)		
Per cent area exceeding -0.1 cm s^{-1}	**0.42**	1.64
Per cent area exceeding $+0.1$ cm s^{-1}	**0.40**	1.44
Total per cent area exceeding ± 0.1 cm s^{-1}	**0.82**	3.08
Major semi-axis (relative)		
Per cent area exceeding -5%	**1.14**	2.52
Per cent area exceeding $+5\%$	**1.14**	12.26
Total per cent area exceeding $\pm 5\%$	**2.28**	14.78
Major semi-axis phase (°)		
Per cent area exceeding $-2.0°$	**0.85**	4.15
Per cent area exceeding $+2.0°$	**0.92**	3.30
Total per cent area exceeding $\pm 2.0°$	**1.77**	7.45
Eccentricity		
Per cent area exceeding -0.04	**0.48**	2.71
Per cent area exceeding $+0.04$	**0.14**	1.26
Total per cent area exceeding ± 0.04	**0.62**	3.97
Major semi-axis direction (°)		
Per cent area exceeding $-5.0°$	**0.45**	1.78
Per cent area exceeding $+5.0°$	**0.34**	1.58
Total per cent area exceeding $\pm 5.0°$	**0.79**	3.36

relaxes the required node spacing over the continental shelf, mirroring resolution requirements of one-dimensional LTEA-based grids [13,14].

The methodologies presented herein for two-dimensional finite element grids based on an LTEA warrant consideration by coastal ocean circulation modelers and may be extended to other areas of grid generation and modeling. The error comparisons of Figures 8–10 and Tables I and II show the LTEA-based grid to be significantly superior to the wavelength-to-gridsize ratio mesh for these linear simulations. Further, the LTEA-based approach permits an *a posteriori* (i.e., after the performance of a preliminary linear simulation) assimilation of large bathymetric datasets by using a fine-resolution mesh. As a result of the preliminary simulation, important bathymetric features are recognized and integrated into the unstructured finite element grid.

The LTEA-based procedure lays the groundwork for an automatic production of accurate, efficient finite element grids for shallow water modeling. Future work must determine the effect that a combination of multiple tidal constituents, non-linear bottom friction, Coriolis, and tidal potential terms has on the LTEA and, subsequently, the final mesh design. Subsequent efforts can then focus on a dynamic application of the LTEA-based approach to an existing unstructured grid, which will enhance the solution of more general shallow-water problems that require adaptive in time mesh refinement (e.g., hurricane storm surge calculations).

REFERENCES

1. Lynch DR, Gray WG. A wave equation model for finite element tidal computations. *Computer in Fluids* 1979; **7**: 207–228.
2. Lynch DR. Progress in hydrodynamic modeling, review of US contributions, 1979–1982. *Review of Geophysical Space Physics* 1983; **21**: 741–754.
3. Kinnmark IPE. The shallow water wave equations: formulation, analysis and application. PhD dissertation, Department of Civil Engineering, Princeton University, NJ, 1984.
4. Westerink JJ, Gray WG. Progress in surface water modeling. *Review in Geophysics* 1991; **29**: 210–217.
5. Luettich RA Jr, Westerink JJ, Scheffner NW. ADCIRC: an advanced three-dimensional circulation model for shelves, coasts and estuaries. Report 1: theory and methodology of ADCIRC-2DDI and ADCIRC-3DL. Technical Report DRP-92-6, Department of the Army, 1992.
6. Foreman MGG. An accuracy analysis of boundary conditions for the forced shallow water equations. *Journal of Computational Physics* 1986; **64**: 334–367.
7. Westerink JJ, Luettich RA Jr, Wu JK, Kolar RL. The influence of normal flow boundary conditions on spurious modes in finite element solutions to the shallow water equations. *Internatioanl Journal for Numerical Methods in Fluids* 1994; **18**: 1021–1060.
8. Kolar RL, Gray WG, Westerink JJ. Boundary conditions in shallow water models—an alternative implementation for finite element codes. *International Journal for Numerical Methods in Fluids* 1996; **22**: 603–618.
9. Blain CA, Westerink JJ, Luettich RA Jr. The influence of domain size on the response characteristics of a hurricane storm model. *Journal of Geophysical Research* 1994; **99**(C9): 18467–18479.
10. Westerink JJ, Luettich RA Jr, Muccino JC. Modeling tides in the western North Atlantic using unstructured graded grids. *Tellus* 1994; **46A**: 178–199.
11. Westerink JJ, Muccino JC, Luettich RA Jr. Resolution requirements for a tidal model of the Western North Atlantic and Gulf of Mexico. In *Proceedings of the IX International Conference on Computational Methods in Water Resources*, Russell TF Jr, *et al.* (eds). Computational Mechanics Publications: Southampton, UK, 1992.
12. Luettich RA Jr, Westerink JJ. Continental shelf scale convergence studies with a barotropic tidal model. In *Quantitative Skill Assessment for Coastal Ocean Models*, vol. 47, Lynch DR, Davies AM Jr (eds). American Geophysical Union: Washington, DC, 1995; 349–371.
13. Hagen SC. Finite element grids based on a localized truncation error analysis. PhD dissertation, Department of Civil Engineering and Geological Sciences, University of Notre Dame, IN, 1998.
14. Hagen SC, Westerink JJ, Kolar RL. One-dimensional finite element grids based on a localized truncation error analysis. *International Journal for Numerical Methods in Fluids* 2000; **32**: 241–261.
15. Westerink JJ, Blain CA, Luettich RA Jr, Scheffner NW. ADCIRC: an advanced three-dimensional circulation model for shelves, coasts and estuaries. Report 2: user's manual for ADCIRC-2DDI. Technical Report DRP-92-6, Department of the Army, 1994.
16. Westerink JJ, Luettich RA Jr, Scheffner NW. ADCIRC: an advanced three-dimensional circulation model for shelves, coasts and estuaries. Report 3: development of a tidal constituent database for the western North Atlantic and Gulf of Mexico. Technical Report DRP-92-6, Department of the Army, 1993.
17. Horstmann O. Adaptive grids for hydroengineering based upon predefined construction segments. In *Advances in Hydro-Science and -Engineering*, vol. III, Holz KP, Bechteler W, Wang SSY, Kawahar M (eds). The University of Mississippi: Oxford, MS, 1998.
18. Burnett DS. *Finite Element Analysis from Concepts to Applications*. Addison-Wesley Publishing: Reading, MA, 1988.